# Electrostatic Manifestation of Micro-Heterogeneous Solvation Structures in Deep-Eutectic Solvents: A Spectroscopic Approach

Srijan Chatterjee, Tapas Haldar, Deborin Ghosh, and Sayan Bagchi*

ACCESS | Metrics & More | Article Recommendations | SI Supporting Information

**ABSTRACT:** Deep eutectic solvents have emerged as inexpensive green alternatives to conventional solvents for diverse applications in chemistry and biology. Despite their importance as useful media in various applications, little is known about the microscopic solvation structures of deep eutectic solvents around solutes. Herein, we show that the electrostatic field, which can be estimated both from infrared experiments and theory, can act as a unified concept to report on the microscopic heterogeneous solvation of deep eutectic solvents. Using a fluorophore containing the carbonyl moiety as the solute and the electrostatic field as a descriptor of the solvation structure of the deep eutectic solvents, we report the residue-specific distribution, orientation, and hydrogen bonding in deep eutectic solvents constituting of choline chloride and alcohols of varying chain-lengths. We observe that an increase in alcohol chain-length not only affects the alcohol's propensity to form hydrogen bond to the solute but also alters the spatial arrangement of choline cations around the solute, thereby leading to a microheterogeneity in the solvation structure. Moreover, to extend our electrostatic field based strategy to other deep eutectic solvents, we report an emission spectroscopy based method. We show that this method can be applied, in general, to all deep eutectic solvents, irrespective of their constituents. Overall, this work integrates experiments with molecular dynamics simulations to provide insights into the heterogeneous DES solvation.
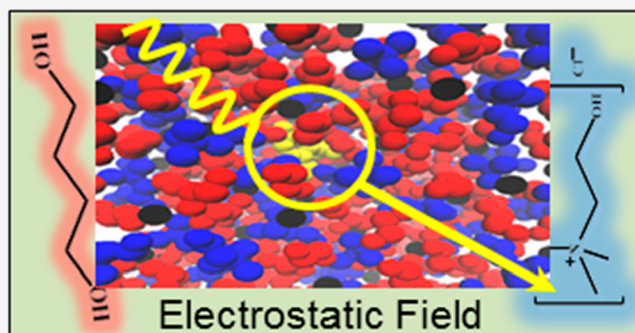
## INTRODUCTION

Deep eutectic solvent (DES), a neoteric class of environmentally benign solvents, has gained significant popularity as a suitable alternative to organic solvents.[1−3] A typical DES consists of two or more components mixed in a certain mole ratio, with at least one hydrogen bond acceptor (HBA) and a hydrogen bond donor (HBD).[2−4] DES, owing to extensive interspecies HB interactions, shows a large depression in melting point which allows the formation of a stable solvent at the room temperature.[2,3] Commonly used DESs are composed of quaternary ammonium salts like choline chloride (ChCl) as the HBA and amides, alcohols, and acids as the HBD. The green character of DES has attracted potential applications in diverse fields of chemistry and biology which include organic synthesis,[5,6] catalysis,[7,8] biotransformations,[9,10] and nanoscience[11,12] among many others. Moreover, protein stability[13−15] and enzyme activity[16,17] have been successfully explored in DES as an alternative to water.

In recent times, studies have been performed to unravel heterogeneous nature of deep eutectic microstructure both from spectroscopic and computational standpoint.[18−25] The effect of the hydrogen bonding partner on DES property and its relation with nanoscale heterogeneity has been analyzed using classical MD simulation[19,26,27] and ab initio MD simulation.[28,29] Microscopic structure and solute−DES inter-

action are also discussed in conjunction with the polarity of the HBD partner.[30−35] A few recent interesting studies also discuss the stability of DES in the aqueous presence of water.[27,36,37]

As the choice of an appropriate DES for any given process depends on the DES solvation properties, insights into the DES solvation structures around a solute is desired.[32,38,39] Alcohol-based (as HBD) eutectic systems are used as media in various applications due to their significantly low viscosity compared to other DESs.[32,40] It has been suggested that changes in the hydrocarbon chain-length of the alcohol significantly influence the properties of alcohol-based DES.[30,41] However, little is known about how the residue specific distribution and the hydrogen bonding of the DES constituents (ChCl and alcohol) are altered by the alcohol chain length. Thus, it is critical to obtain a molecular understanding of how the solvation structures of alcohol-based DES with varying chain-lengths influence the solute−
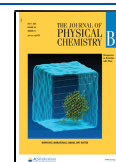
solvent interactions. To gauge solute−solvent interactions, spectroscopic responses of fluorophores have been commonly used to assess the polarity of DES through semiempirical polarity scales.[35,40,42−44] Although these studies are informative, the continuum semiempirical polarity parameters do not account for the microscopic nature of the solvent. Moreover, these parameters cannot be computed from simulations and thus cannot provide the microscopic details of the DES solvation structures. To overcome this limitation, we require an experimental, yet microscopic, observable of solute−solvent interactions, which can independently be estimated from simulations.

It has been recently shown that electrostatic field $(\vec{F})$ can serve as a quantitative and microscopic descriptor of solute−solvent interactions in neat solvents and solvent mixtures.[45,46] Carbonyl (C=O) groups, ubiquitous in chemistry and biology, has been reported to show a linear correlation between the C=O infrared (IR) frequencies $(\bar{v}_{C=O})$ and the corresponding electrostatic fields $(\vec{F}_{C=O}$ along the C=O bond through vibrational Stark effect (VSE).[47,48] As $\vec{F}_{C=O}$ depends both on the distances of all other solvent atoms from the C=O and the residual partial charges on each solvent atom, it can be directly mapped to the DES solvation structure. Moreover, $\vec{F}_{C=O}$ exerted by the DES on the solute's C=O can be independently estimated from molecular dynamics (MD) simulations. The electrostatic field estimated from simulations can be compared with that measured from experiment to benchmark the MD force fields.[47] A good agreement between the common microscopic parameter $(\vec{F}_{C=O})$ obtained independently from experiments and simulations would allow us to get insights into the variation in the solvation structures of alcohol-based DES with varying chain lengths.

In this report, we have experimentally determined $\vec{F}_{C=O}$ along the C=O bond of a fluorophore, coumarin 151 (C151), exerted by the four alcohol-based DESs (Scheme 1) from

**Scheme 1. Molecular Structures of the Constituents of the DES Used in This Study**
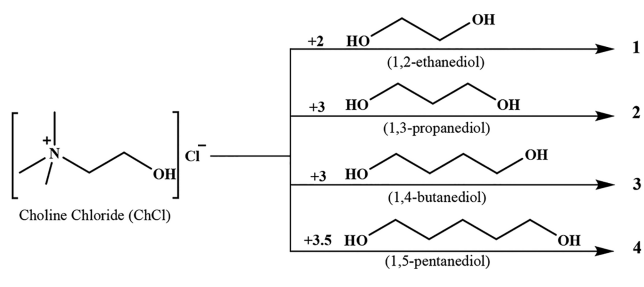


infrared (IR) spectroscopy. We have compared the experimentally determined $\vec{F}_{C=O}$ with those estimated from MD simulations. Furthermore, we have decomposed the total electrostatic field into contributions from individual HBA and HBD constituents to obtain an in-depth understanding of the microscopic heterogeneous solvation of the DESs around the solute molecule. Moreover, in order to obtain a general strategy for $\vec{F}_{C=O}$ estimation in any DES, irrespective of its constituents, we have successfully used the emission peak maxima of the fluorophore to estimate electrostatic fields in three non-alcohol-based DESs.

## ■ MATERIALS AND METHODS

**Materials.** Coumarin151(C151), choline chloride (ChCl), 1,2-ethanediol, 1,3-propanediol, 1,4-butanediol, 1,5-pentanediol, urea, malonic acid, and oxalic acid and solvents like dibutyl ether (DBE), diethyl ether (DEE), tetrahydrofuran (THF), valeronitrile (VLN), and acetonitrile (ACN) were purchased from Sigma-Aldrich. All chemicals other than ChCl were used without further purification. Milli-Q water was used in this study.

**Sample Preparation.** All of the deep eutectic solvents were synthesized by following a reported procedure.[41,49] Choline chloride was dried in a vacuum oven at 90 °C for 24 h before use. All of the deep eutectic solvents were prepared in an argon-filled glovebox. ChCl were mixed with respective diols, urea and acids with a specific molar ratio. Then the mixtures were heated and stirred at 60−70 °C until fully homogeneous colorless liquids were formed. The reaction mixture was allowed to cool to room temperature before any measurements were taken. Water content was measured by using a Metrohm Karl Fischer titrator and results indicated that water contents are less than 0.5% by weight (Table S1). Full IR absorption spectra of DESs are shown in Figure S1 (Supporting Information). The absence of the water band (OH bend) near 1700 cm$^{-1}$ in pure DES spectra as compared to that in pure water and DES water mixtures (2:1 v/v) (Figure S2, Supporting Information)) validates the results obtained from water content measurement in DESs.

**Spectroscopy.** IR absorption spectra were recorded on a FTIR-Bruker Vertex 70 spectrometer with 2 cm$^{-1}$ resolution at room temperature. For each sample, ∼60 μL of the sample solution was loaded into a demountable cell consisting of two windows (CaF$_2$, 3 mm thickness, Shenzen Laser), separated by a mylar spacer of 56 μm thickness. IR cells were prepared in Argon filled glovebox to minimize the water contamination. Fluorescence was obtained with a calibrated Spectrofluorometer FS5 (Edinburgh Instruments).

**Molecular Dynamics Simulations.** Classical molecular dynamics simulations were performed by GROMACS 2016.5 package.[50] Parameters for pure solvents and coumarin 151 dye were taken from our previous work based on AMBER framework.[51] Force field parameters for ChCl, 1,2-ethanediol, urea, malonic acid, and oxalic acid are taken from the work of Brian et al.,[26] and for 1,3-propanediol and 1,4-butanediol, we have used force field parameters for alcohol generated by the automatic server by Jorgensen and co-workers.[52] Cubic simulation boxes are defined by 100 choline chloride ion pair and varying number of hydrogen bond donor according to the experimental mole fraction using GROMACS build in tool. Prior to each simulation step, we have performed energy minimization by steepest descent algorithm with 2 fs step size. NVT ensemble was performed at 300 K for 1 ns with a velocity rescale thermostat and was followed by the NPT ensemble at 300 K temperature and 1 bar pressure using a Parrinello−Rahman barostat for 5 ns. LINCS is used to constrain all the hydrogen atoms which are covalently bonded. Production runs are carried out for a minimum of 10 ns.
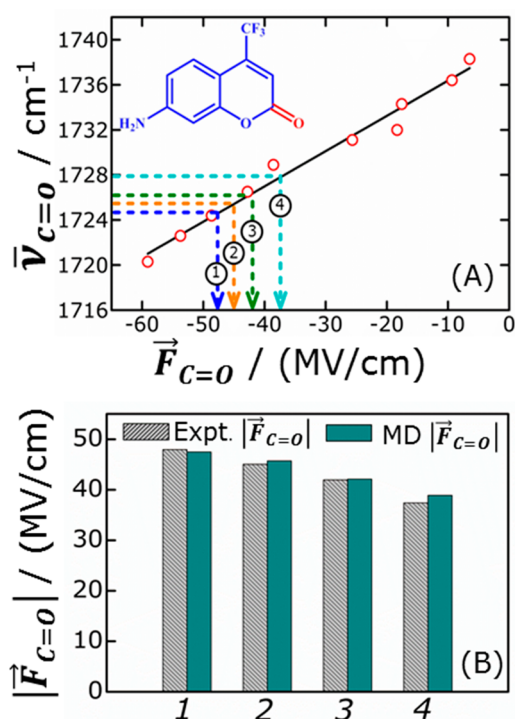
Hydrogen bond analysis are performed on GROMACS of last 5 ns of trajectory where position outputs are saved every 500 ps. The distance cutoff of 3.5 Å and angle cutoff of 30° are used for the hydrogen bond calculation. Represented snapshots are obtained by using GROMACS cluster analysis tool to get the most probable arrangement. Electric field on carbonyl

bonds of coumarin151 have been calculated according to our previous work.[48]

## RESULTS AND DISCUSSION

Coumarin 151 (C151), a common fluorophore containing an ester C=O moiety is dissolved in the synthesized DESs to perform the spectroscopic experiments. The emission peak positions of C151 in the DESs (Figure S3 in the Supporting Information) are similar to those of C151 in acetonitrile− (ACN−) water mixtures (Figure S4) and show a gradual blue-shift with increasing hydrocarbon chain-length of the alcohols.

The blue-shift in the emission maxima is consistent with an earlier report, albeit using different fluorophores.[32] Furthermore, the IR spectra in the C=O stretch region of C151 are measured in neat solvents and aqueous ACN solutions (Figure S4 in the Supporting Information). The C=O stretch region in C151 shows overlapping transitions (Figure S5A in the Supporting Information) arising from the C=O stretch (lower frequencies) and Fermi resonance peaks (higher frequencies).[53] The peaks are deconvolved to obtain the C=O peak positions ($\overline{\nu}_{C=O}$), as shown in Figure S5B in the Supporting Information. A gradual red-shift in $\overline{\nu}_{C=O}$ is observed with the increasing polarity of the solvents. We have also estimated $\vec{F}_{C=O}$ from MD simulations in the same solvents and aqueous ACN solutions.[54] A plot of the paired points ($\overline{\nu}_{C=O}, \vec{F}_{C=O}$) shows a linear correlation ($R^2 = 0.98$) with a slope of 0.32 cm$^{-1}$/(MV/cm) (Figure 1A). This is in excellent agreement with the reported Stark tuning rates [$\Delta\overline{\nu}_{C=O}/\Delta\vec{F}_{C=O} \sim 1.0$ cm$^{-1}$/(MV/cm)] of ester C=O,[55] independently measured from vibrational Stark spectroscopy, containing a local field

factor of ∼3.[56] The best-fit straight line in Figure 1A acts as a calibration line and allows us to estimate $\vec{F}_{C=O}$ using the experimentally measured $\overline{\nu}_{C=O}$ in any unknown environment.[47] To estimate the average electrostatic fields exerted along the solute C=O bond by the alcohol-based DESs with varying hydrocarbon chain-lengths, we obtain the values of $\overline{\nu}_{C=O}$ of C151 in **1**, **2**, **3**, and **4** (Figure S6 in the Supporting Information). Similar to the emission peak maxima, $\overline{\nu}_{C=O}$ also show a gradual blue-shift with increasing hydrocarbon chain-length of the alcohols. Using, the calibration line in Figure 1A, we estimate the fields to be −47.9, −45.1, −41.9, and −37.4 MV/cm in **1**, **2**, **3**, and **4**, respectively. This result indicates that $\vec{F}_{C=O}$ exerted by the DES decreases with the increase in the chain-length of the alcohols, plausibly due the increase in hydrophobicity arising from the longer hydrocarbon chains. Furthermore, we have generated the force-fields for **1**, **2**, **3**, and **4** and performed MD simulations to predict $\vec{F}_{C=O}$ on C151 in the four alcohol-based DESs. Figure 1B and Table S1 in the Supporting Information show that the $\vec{F}_{C=O}$ estimated from the IR spectra are in excellent agreement with those predicted from MD simulations.

As the IR estimated electrostatic fields are validated by the independently measured Stark tuning rate (from the slope in Figure 1A), this agreement between theory and experiment allows us to obtain further insights about the variation in HB, distribution, and orientation of the DES constituents around C151 as a function of alcohol chain-length. First, we have decomposed the total $\vec{F}_{C=O}$ estimated from MD simulations to the contributions from the individual constituents (HBA and HBD) for all the alcohol-based DESs (Figure 2A and Table S2
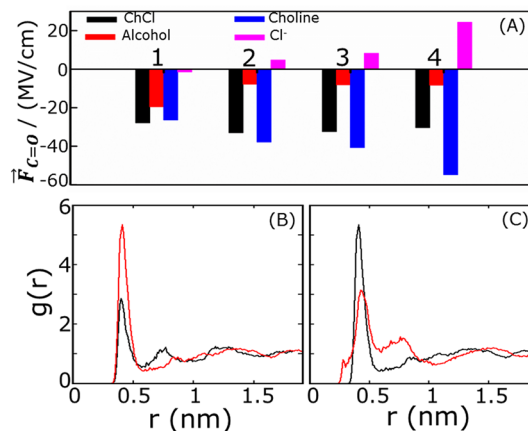


**Figure 2.** (A) Contributions from ChCl, alcohol, choline cation, and chloride anion to the total $\vec{F}_{C=O}$. (B) RDF between the C=O oxygen of C151 and the choline nitrogen in 1,2-ethanediol (**1**, black) and 1,5-pentanediol (**4**, red). (c) RDF between the C=O oxygen of C151 and the choline nitrogen in 1,5-pentanediol (**4**, black) and between the C=O oxygen of C151 and the choline oxygen in 1,5-pentanediol (**4**, red).



**Figure 1.** (A) C=O IR stretching frequencies ($\overline{\nu}_{C=O}$) in neat solvents and ACN-water mixtures show a linear correlation with the corresponding $\vec{F}_{C=O}$ of C151. The black line indicates the best fit line ($R^2 = 0.98$). $\vec{F}_{C=O}$ in **1**, **2**, **3**, and **4** are estimated from their respective $\overline{\nu}_{C=O}$. (B) Bar plots of IR estimated and MD predicted $\vec{F}_{C=O}$ in **1**, **2**, **3**, and **4** show excellent agreement.

in the Supporting Information). It is observed that the exerted field arises predominantly (60−80%) from ChCl across all DESs. Despite the apparent change in hydrophobicity with the variation in alcohol chain-length, the diols have a smaller contribution to the overall $\vec{F}_{C=O}$ experienced by the solute. The largest contribution of the alcohol constituent is observed in **1**; the electrostatic field (a greater negative indicates larger stabilization) drops off to about half the value in **1** for larger chain alcohols. However, the electrostatic fields exerted by

ChCl almost remain constant and no apparent trend can be observed in as a function of alcohol chain-length. When we further decompose the total field arising from ChCl field into contributions from the choline cations and the chloride anions (Figure 2A and Table S2 in the Supporting Information), we find an interesting trend. A monotonic increase in the stabilizing field from the choline cations (C=O-cation attraction) as a function of increasing alcohol chain-length is accompanied by a subsequent increase in the destabilizing field from the chloride anions (C=O−anion repulsion). This result suggests ChCl remains as an ion-pair, as also reported in a recent study.[57] Furthermore, as the electrostatic field is inversely proportional to the square of the distance, the result indicates that the choline concentration around the C151 C=O increases with increase in the chain-length of the alcohol constituent. To obtain a greater insight into this, radial distribution function (RDF) is calculated between the C=O oxygen (O) of C151 and the choline nitrogen (N) for all DESs. As surmised from the changes in the electrostatic fields exerted by choline in the alcohol-based DESs, we observe that the RDF peak intensity increases with increase in the alcohol chain-length (Figure 2B). The variation in the RDF peak intensities for different alcohol chain-lengths correlates with the variation observed in $\vec{F}_{C=O}$ exerted by choline. Additionally, to investigate the orientation of the choline molecules with respect to the solute C=O, we have calculated the RDF between the carbonyl oxygen of C151 and the choline O in in 1, 2, 3, and 4. Figure 2C shows that the N atom of the choline cation is predominantly oriented toward the solute carbonyl. The small peak in the RDF between C=O oxygen and choline O within 3.5 Å indicates a small population of the choline cation where the hydroxyl groups are oriented toward the solute C=O, plausibly forming HB to the C=O. As both the choline and the alcohol constituents of the DESs contain OH groups it will be interesting to understand which is the preferred hydrogen bond partner to C151 C=O. We have performed hydrogen bond analysis, and it demonstrates that preferential hydrogen bonding occurs between C151 C=O and alcohol OH (Table S3 in the Supporting Information). However, the HB propensity monotonically decreases with increase in the alcohol chain-length. Thus, it can be concluded that the increase in alcohol chain-length not only perturbs the HB affinity but it also affects the spatial arrangement of choline cation around the solute leading to a microheterogeneity in the solvation structure. The overall solvation environment is manifested in the total $\vec{F}_{C=O}$ experienced by the solute C=O, however, decomposition of the total field into residue-specific contributions unfolds the microheterogeneity of the solvation structure. Representative MD snapshots in Figure 3 show the heterogeneous solvation structure around the solute in four different alcohol-based DESs with varying chain length.

Even though we have established an electrostatic field based methodology to obtain molecular insights into the solvation structure of DES, this strategy requires experimental determination of $\overline{v}_{C=O}$ from the IR spectra to estimate the electrostatic fields exerted of the solute. However, the HBD constituent of DES is not restricted to alcohols. Amides and carboxylic acids, which have also been reported as common HBD constituents in DESs, themselves contain the C=O group. As it is not feasible to decipher $\overline{v}_{C=O}$ of the solute in the presence of the broad and intense IR signal from the solvent C=O group, our strategy is limited to alcohol-based DES. In search of an alternate strategy applicable to all DES, we
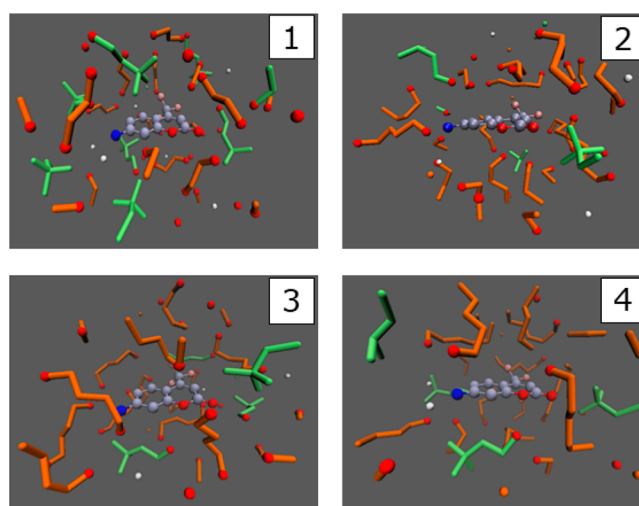


**Figure 3.** Representative snapshots of **1**, **2**, **3**, and **4** from MD trajectories. The snapshots are obtained by averaging the coordinates of a 5 ns long simulation.

decided to plot $\overline{v}_{C=O}$ of **1**, **2**, **3**, and **4** against the corresponding emission frequencies (Figure 4A) as both
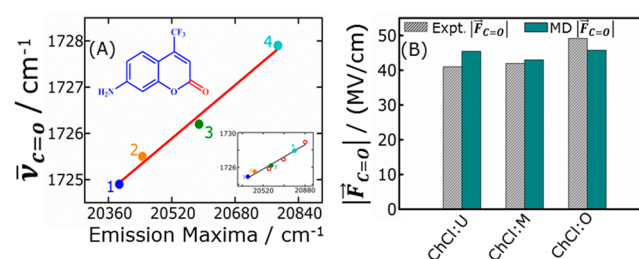


**Figure 4.** (A) C=O IR stretching frequencies ($\overline{v}_{C=O}$) in **1**, **2**, **3**, and **4** and aqueous acetonitrile solutions (v/v) {80% acetonitrile, 60% acetonitrile, 40% acetonitrile} [red circle, inset] show a linear correlation with the corresponding emission peak maxima of C151. The red line indicates the best fit line ($R^2 = 0.98$). (B) Bar plot of $\vec{F}_{C=O}$ estimated from emission peak maxima and MD simulations in Chcl:U, ChCl:M, and ChCl:O show good agreement

emission and IR peak maxima in alcohol-based DESs show blue shifts with increasing chain length. Interestingly, a linear correlation ($R^2 = 0.98$) is observed between $\overline{v}_{C=O}$ and the emission peak maxima. As the other commonly used DESs contain a C=O moiety, they cannot be used to check the generality of this linear relation between $\overline{v}_{C=O}$ and the emission frequencies. However, when points from noneutectic solutions, containing a HBD and a HBA (binary mixtures of ACN and water), are included (Figure 4A, inset), the excellent linear correlation ($R^2 = 0.97$) between $\overline{v}_{C=O}$ and the emission peak maxima validates the generality of the aforesaid linearity. This observation implies that $\vec{F}_{C=O}$ can also be estimated using the emission peak maxima. The origin of this linear relationship is itself an interesting topic of investigation, however, it falls outside the scope of this work. Instead, we have compared the experimental $\vec{F}_{C=O}$ from emission peak maxima with those estimated from simulations to inspect the generality of this approach for DES constituents containing the C=O group.

Combining the linear relationships from Figures 1A and 4A, we have estimated $\vec{F}_{C=O}$ in three more DESs (Scheme 2): **5**

**Scheme 2. Molecular Structures of Other Constituents of the DES Used in This Study**
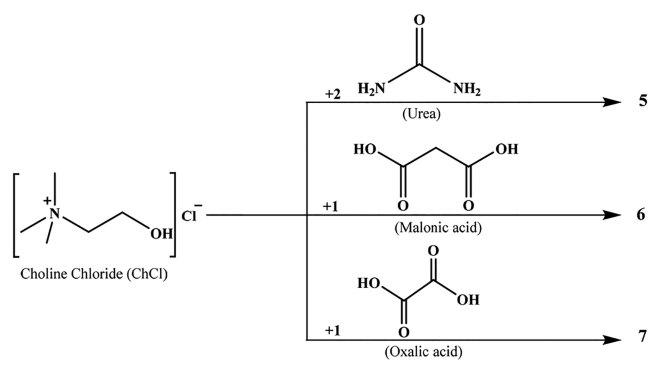


(ChCl:U), **6** (ChCl:M), and **7** (ChCl:O), where the HBD constituents contain the C=O group. The estimated values of $\vec{F}_{C=O}$ on C151 in these three DESs are given in Table S4 in the Supporting Information. Furthermore, we have independently predicted $\vec{F}_{C=O}$ in these C=O-containing DESs from MD simulations. Figure 4B shows that the experimentally estimated fields agree well with the MD predicted fields. This agreement demonstrates that a molecular level understanding of the DES solvation structures can indeed be obtained for other DESs using the electrostatic field based approach, independent of the DES constituents.

## CONCLUSION

To understand changes in solute–solvent interactions in different DESs, earlier reports assessed empirical solvent parameters depicting polarity, HBD acidity, and HBA basicity using responses of fluorescent probes.[21,31,34,35] However, these empirical parameters cannot be computed from MD simulations, and thus they cannot provide further insights into the heterogeneous solvation structure of the DES. We have successfully demonstrated that electrostatic field can be used a unified concept to decipher the microheterogeneity as well as the subtle changes in the solvation structures of the alcohol-based DESs with varying hydrocarbon chain length. We have obtained a molecular understanding of the distribution, orientation, and HB of the constituents with respect to DES solvation. Furthermore, we have shown that an emission spectroscopy based methodology allows us to determine the electrostatic fields in any DES, irrespective of the constituents. Recent experimental and theoretical studies have shown that electrostatic fields play key roles in chemical and enzymatic processes.[58–60] This electrostatic field based strategy will enable us to connect theoretical and experimental results and to provide insights into the various applications of DES in chemistry and biology.

## ASSOCIATED CONTENT

### Supporting Information

The Supporting Information is available free of charge at https://pubs.acs.org/doi/10.1021/acs.jpcb.9b11352.

> Figures showing FTIR spectra, emission spectra, fluorescence emission spectra, IR absorption spectra, and radial distribution functions and tables of spectral data, deconvolution of total electric field, calculated number of hydrogen bonds, and emission maxima (PDF)

## AUTHOR INFORMATION

### Corresponding Author

**Sayan Bagchi** − *Physical and Materials Chemistry Division, CSIR-National Chemical Laboratory (CSIR-NCL), Pune 411008, India; Academy of Scientific and Innovative Research (AcSIR), Ghaziabad 201002, India;* ⊙ orcid.org/0000-0001-6932-3113; Phone: +91-20-25903048; Email: s.bagchi@ncl.res.in; Fax: +91-20-25902636

### Authors

**Srijan Chatterjee** − *Physical and Materials Chemistry Division, CSIR-National Chemical Laboratory (CSIR-NCL), Pune 411008, India; Academy of Scientific and Innovative Research (AcSIR), Ghaziabad 201002, India*

**Tapas Haldar** − *Physical and Materials Chemistry Division, CSIR-National Chemical Laboratory (CSIR-NCL), Pune 411008, India; Academy of Scientific and Innovative Research (AcSIR), Ghaziabad 201002, India*

**Deborin Ghosh** − *Physical and Materials Chemistry Division, CSIR-National Chemical Laboratory (CSIR-NCL), Pune 411008, India*

Complete contact information is available at:
https://pubs.acs.org/10.1021/acs.jpcb.9b11352

### Notes

The authors declare no competing financial interest.

## ACKNOWLEDGMENTS

## REFERENCES

(1) Francisco, M.; van den Bruinhorst, A.; Kroon, M. C. Low-transition-temperature Mixtures (LTTMs): A New Generation of Designer Solvents. *Angew. Chem., Int. Ed.* **2013**, *52*, 3074−3085.

(2) Smith, E. L.; Abbott, A. P.; Ryder, K. S. Deep eutectic solvents (DESs) and their applications. *Chem. Rev.* **2014**, *114* (21), 11060−11082.

(3) Zhang, Q.; De Oliveira Vigier, K.; Royer, S.; Jerome, F. Deep eutectic solvents: syntheses, properties and applications. *Chem. Soc. Rev.* **2012**, *41* (21), 7108−7146.

(4) Abbott, A. P.; Boothby, D.; Capper, G.; Davies, D. L.; Rasheed, R. K. Deep Eutectic Solvents Formed Between Choline Chloride and Carboxylic Acids: Versatile Alternatives to Ionic Liquids. *J. Am. Chem. Soc.* **2004**, *126* (29), 9142−7.

(5) Alonso, D. A.; Baeza, A.; Chinchilla, R.; Guillena, G.; Pastor, I. M.; Ramón, D. J. Deep Eutectic Solvents: The Organic Reaction Medium of the Century. *Eur. J. Org. Chem.* **2016**, *2016* (4), 612−632.

(6) Ruß, C.; König, B. Low melting mixtures in organic synthesis - an alternative to ionic liquids? *Green Chem.* **2012**, *14* (11), 2969−2982.

(7) Abbott, A. P.; Capper, G.; Davies, D. L.; Rasheed, R. K.; Tambyrajah, V. Quaternary ammonium zinc- or tin-containing ionic liquids: water insensitive, recyclable catalysts for Diels-Alder reactions. *Green Chem.* **2002**, *4* (1), 24−26.

(8) Gu, Y.; Jérôme, F. Bio-based solvents: an emerging generation of fluids for the design of eco-efficient processes in catalysis and organic chemistry. *Chem. Soc. Rev.* **2013**, *42* (24), 9550−9570.

(9) Dominguez de Maria, P.; Maugeri, Z. Ionic liquids in biotransformations: from proof-of-concept to emerging deep-eutectic-solvents. *Curr. Opin. Chem. Biol.* **2011**, *15* (2), 220−225.

(10) Gorke, J. T.; Srienc, F.; Kazlauskas, R. J. Hydrolase-catalyzed biotransformations in deep eutectic solvents. *Chem. Commun.* **2008**, No. 10, 1235−1237.

(11) Liao, H.-G.; Jiang, Y.-X.; Zhou, Z.-Y.; Chen, S.-P.; Sun, S.-G. Shape-Controlled Synthesis of Gold Nanoparticles in Deep Eutectic Solvents for Studies of Structure-Functionality Relationships in Electrocatalysis. *Angew. Chem.* **2008**, *120* (47), 9240−9243.

(12) Wagle, D. V.; Zhao, H.; Baker, G. A. Deep eutectic solvents: sustainable media for nanoscale and functional materials. *Acc. Chem. Res.* **2014**, *47* (8), 2299−2308.

(13) Esquembre, R.; Sanz, J. M.; Wall, J. G.; del Monte, F.; Mateo, C. R.; Ferrer, M. L. Thermal unfolding and refolding of lysozyme in deep eutectic solvents and their aqueous dilutions. *Phys. Chem. Chem. Phys.* **2013**, *15* (27), 11248−11256.

(14) Monhemi, H.; Housaindokht, M. R.; Moosavi-Movahedi, A. A.; Bozorgmehr, M. R. How a protein can remain stable in a solvent with high content of urea: insights from molecular dynamics simulation of Candida antarctica lipase B in urea: choline chloride deep eutectic solvent. *Phys. Chem. Chem. Phys.* **2014**, *16* (28), 14882−14893.

(15) Parnica, J.; Antalik, M. Urea and guanidine salts as novel components for deep eutectic solvents. *J. Mol. Liq.* **2014**, *197*, 23−26.

(16) Harifi-Mood, A. R.; Ghobadi, R.; Divsalar, A. The effect of deep eutectic solvents on catalytic function and structure of bovine liver catalase. *Int. J. Biol. Macromol.* **2017**, *95*, 115−120.

(17) Wu, B. P.; Wen, Q.; Xu, H.; Yang, Z. Insights into the impact of deep eutectic solvents on horseradish peroxidase: Activity, stability and structure. *J. Mol. Catal. B: Enzym.* **2014**, *101*, 101−107.

(18) Mjalli, F. S.; Naser, J.; Jibril, B.; Alizadeh, V.; Gano, Z. Tetrabutylammonium Chloride Based Ionic Liquid Analogues and Their Physical Properties. *J. Chem. Eng. Data* **2014**, *59* (7), 2242−2251.

(19) Kaur, S.; Malik, A.; Kashyap, H. K. Anatomy of Microscopic Structure of Ethaline Deep Eutectic Solvent Decoded through Molecular Dynamics Simulations. *J. Phys. Chem. B* **2019**, *123* (39), 8291−8299.

(20) Dou, J.; Zhao, Y.; Yin, F.; Li, H.; Yu, J. Mechanistic Study of Selective Absorption of NO in Flue Gas Using EG-TBAB Deep Eutectic Solvents. *Environ. Sci. Technol.* **2019**, *53* (2), 1031−1038.

(21) Das, A.; Biswas, R. Dynamic Solvent Control of a Reaction in Ionic Deep Eutectic Solvents: Time-Resolved Fluorescence Measurements of Reactive and Nonreactive Dynamics in (Choline Chloride + Urea) Melts. *J. Phys. Chem. B* **2015**, *119* (31), 10102−10113.

(22) Guchhait, B.; Das, S.; Daschakraborty, S.; Biswas, R. Interaction and dynamics of (alkylamide + electrolyte) deep eutectics: Dependence on alkyl chain-length, temperature, and anion identity. *J. Chem. Phys.* **2014**, *140* (10), 104514.

(23) Das, A.; Das, S.; Biswas, R. Density relaxation and particle motion characteristics in a non-ionic deep eutectic solvent (acetamide + urea): Time-resolved fluorescence measurements and all-atom molecular dynamics simulations. *J. Chem. Phys.* **2015**, *142* (3), 034505.

(24) Das, A.; Das, S.; Biswas, R. Fast fluctuations in deep eutectic melts: Multi-probe fluorescence measurements and all-atom molecular dynamics simulation study. *Chem. Phys. Lett.* **2013**, *581*, 47−51.

(25) Mukherjee, K.; Das, A.; Choudhury, S.; Barman, A.; Biswas, R. Dielectric Relaxations of (Acetamide + Electrolyte) Deep Eutectic Solvents in the Frequency Window, 0.2 ≤ ν/GHz ≤ 50: Anion and Cation Dependence. *J. Phys. Chem. B* **2015**, *119* (25), 8063−8071.

(26) Doherty, B.; Acevedo, O. OPLS Force Field for Choline Chloride-Based Deep Eutectic Solvents. *J. Phys. Chem. B* **2018**, *122* (43), 9982−9993.

(27) Kumari, P.; Shobhna; Kaur, S.; Kashyap, H. K. Influence of Hydration on the Structure of Reline Deep Eutectic Solvent: A Molecular Dynamics Study. *ACS Omega* **2018**, *3* (11), 15246−15255.

(28) Fetisov, E. O.; Harwood, D. B.; Kuo, I. F. W.; Warrag, S. E. E.; Kroon, M. C.; Peters, C. J.; Siepmann, J. I. First-Principles Molecular Dynamics Study of a Deep Eutectic Solvent: Choline Chloride/Urea and Its Mixture with Water. *J. Phys. Chem. B* **2018**, *122* (3), 1245−1254.

(29) Stefanovic, R.; Ludwig, M.; Webber, G. B.; Atkin, R.; Page, A. J. Nanostructure, hydrogen bonding and rheology in choline chloride deep eutectic solvents as a function of the hydrogen bond donor. *Phys. Chem. Chem. Phys.* **2017**, *19* (4), 3297−3306.

(30) Chatterjee, S.; Ghosh, D.; Haldar, T.; Deb, P.; Sakpal, S. S.; Deshmukh, S. H.; Kashid, S. M.; Bagchi, S. Hydrocarbon Chain-Length Dependence of Solvation Dynamics in Alcohol-Based Deep Eutectic Solvents: A Two-Dimensional Infrared Spectroscopic Investigation. *J. Phys. Chem. B* **2019**, *123* (44), 9355−9363.

(31) Hossain, S. S.; Paul, S.; Samanta, A. Liquid Structure and Dynamics of Tetraalkylammonium Bromide-Based Deep Eutectic Solvents: Effect of Cation Chain Length. *J. Phys. Chem. B* **2019**, *123* (31), 6842−6850.

(32) Hossain, S. S.; Samanta, A. How do the hydrocarbon chain length and hydroxyl group position influence the solute dynamics in alcohol-based deep eutectic solvents? *Phys. Chem. Chem. Phys.* **2018**, *20* (38), 24613−24622.

(33) Pandey, A.; Bhawna; Dhingra, D.; Pandey, S. Hydrogen Bond Donor/Acceptor Cosolvent-Modified Choline Chloride-Based Deep Eutectic Solvents. *J. Phys. Chem. B* **2017**, *121* (16), 4202−4212.

(34) Pandey, A.; Pandey, S. Solvatochromic Probe Behavior within Choline Chloride-Based Deep Eutectic Solvents: Effect of Temperature and Water. *J. Phys. Chem. B* **2014**, *118* (50), 14652−14661.

(35) Pandey, A.; Rai, R.; Pal, M.; Pandey, S. How polar are choline chloride-based deep eutectic solvents? *Phys. Chem. Chem. Phys.* **2014**, *16* (4), 1559−1568.

(36) Hammond, O. S.; Bowron, D. T.; Edler, K. J. The Effect of Water upon Deep Eutectic Solvent Nanostructure: An Unusual Transition from Ionic Mixture to Aqueous Solution. *Angew. Chem., Int. Ed.* **2017**, *56* (33), 9782−9785.

(37) Posada, E.; López-Salas, N.; Jiménez Riobóo, R. J.; Ferrer, M. L.; Gutiérrez, M. C.; del Monte, F. Reline aqueous solutions behaving as liquid mixtures of H-bonded co-solvents: microphase segregation and formation of co-continuous structures as indicated by Brillouin and 1H NMR spectroscopies. *Phys. Chem. Chem. Phys.* **2017**, *19* (26), 17103−17110.

(38) Cui, Y.; Fulfer, K. D.; Ma, J.; Weldeghiorghis, T. K.; Kuroda, D. G. Solvation dynamics of an ionic probe in choline chloride-based deep eutectic solvents. *Phys. Chem. Chem. Phys.* **2016**, *18* (46), 31471−31479.

(39) Baz, J. r.; Held, C.; Pleiss, J. r.; Hansen, N. Thermophysical properties of glyceline-water mixtures investigated by molecular modelling. *Phys. Chem. Chem. Phys.* **2019**, *21* (12), 6467−6476.

(40) Abbott, A. P.; Harris, R. C.; Ryder, K. S.; D'Agostino, C.; Gladden, L. F.; Mantle, M. D. Glycerol eutectics as sustainable solvent systems. *Green Chem.* **2011**, *13* (1), 82−90.

(41) Harris, R. M. *Physical Properties of Alcohol Based Deep Eutectic Solvents*; University of Leicester: 2008.

(42) Dimroth, K.; Reichardt, C.; Siepmann, T.; Bohlmann, F. About Pyridinium N-Phenolic Betaines and Their Use for Characterizing the Polarity of Solvents. *Justus Liebigs Annalen der Chemie* **1963**, *661* (1), 1−37.

(43) Kamlet, M. J.; Abboud, J. L.; Taft, R. W. The solvatochromic comparison method. 6. The $\pi^*$ scale of solvent polarities. *J. Am. Chem. Soc.* **1977**, *99* (18), 6027−6038.

(44) Kamlet, M. J.; Taft, R. W. The solvatochromic comparison method. I. The $\beta$ -scale of solvent hydrogen-bond acceptor (HBA) basicities. *J. Am. Chem. Soc.* **1976**, *98* (2), 377−383.

(45) Deb, P.; Haldar, T.; Kashid, S. M.; Banerjee, S.; Chakrabarty, S.; Bagchi, S. Correlating Nitrile IR Frequencies to Local Electrostatics Quantifies Noncovalent Interactions of Peptides and Proteins. *J. Phys. Chem. B* **2016**, *120* (17), 4034−4046.

(46) Fried, S. D.; Boxer, S. G. Measuring Electric Fields and Noncovalent Interactions Using the Vibrational Stark Effect. *Acc. Chem. Res.* **2015**, *48* (4), 998−1006.

(47) Fried, S. D.; Bagchi, S.; Boxer, S. G. Measuring Electrostatic Fields in Both Hydrogen-Bonding and Non-Hydrogen-Bonding Environments Using Carbonyl Vibrational Probes. *J. Am. Chem. Soc.* **2013**, *135* (30), 11181−11192.

(48) Haldar, T.; Kashid, S. M.; Deb, P.; Kesh, S.; Bagchi, S. Pick and Choose the Spectroscopic Method to Calibrate the Local Electric Field inside Proteins. *J. Phys. Chem. Lett.* **2016**, 7 (13), 2456−2460.

(49) HÃkkinen, R.; Abbott, A. Solvation of carbohydrates in five choline chloride-based deep eutectic solvents and the implication for cellulose solubility. *Green Chem.* **2019**, 21 (17), 4673−4682.

(50) Abraham, M. J.; Murtola, T.; Schulz, R.; Pall, S. r.; Smith, J. C.; Hess, B.; Lindahl, E. GROMACS: High performance molecular simulations through multi-level parallelism from laptops to super-computers. *SoftwareX* **2015**, 1−2, 19−25.

(51) Wang, J.; Wolf, R. M.; Caldwell, J. W.; Kollman, P. A.; Case, D. A. Development and testing of a general amber force field. *J. Comput. Chem.* **2004**, 25 (9), 1157−74.

(52) Dodda, L. S.; Vilseck, J. Z.; Tirado-Rives, J.; Jorgensen, W. L. 1.14*CM1A-LBCC: Localized Bond-Charge Corrected CM1A Charges for Condensed-Phase Simulations. *J. Phys. Chem. B* **2017**, 121 (15), 3864−3870.

(53) Arjunan, V.; Puviarasan, N.; Mohan, S.; Murugesan, P. Fourier transform infrared and Raman spectral assignments and analysis of 7-amino-4-trifluoromethylcoumarin. *Spectrochim. Acta, Part A* **2007**, 67 (5), 1290−1296.

(54) Haldar, T.; Bagchi, S. Electrostatic Interactions Are Key to C$=$O n-$\pi$* Shifts: An Experimental Proof. *J. Phys. Chem. Lett.* **2016**, 7 (12), 2270−2275.

(55) Schneider, S. H.; Boxer, S. G. Vibrational Stark Effects of Carbonyl Probes Applied to Reinterpret IR and Raman Data for Enzyme Inhibitors in Terms of Electric Fields at the Active Site. *J. Phys. Chem. B* **2016**, 120 (36), 9672−9684.

(56) Olson, J. Z.; Schneider, S. H.; Johansson, P. K.; Luk, T. S.; Schlenker, C. W. Stark Tuning Rates of Organic Carbonates Used in Electrochemical Energy Storage Devices. *J. Phys. Chem. C* **2019**, 123 (18), 11484−11492.

(57) Shaukat, S.; Fedotova, M. V.; Kruchinin, S. E.; Bester-Rogac, M.; Podlipnik, C.; Buchner, R. Hydration and ion association of aqueous choline chloride and chlorocholine chloride. *Phys. Chem. Chem. Phys.* **2019**, 21 (21), 10970−10980.

(58) Fried, S. D.; Bagchi, S.; Boxer, S. G. Extreme electric fields power catalysis in the active site of ketosteroid isomerase. *Science* **2014**, 346 (6216), 1510−1514.

(59) Aragonès, A. C.; Haworth, N. L.; Darwish, N.; Ciampi, S.; Bloomfield, N. J.; Wallace, G. G.; Diez-Perez, I.; Coote, M. L. Electrostatic catalysis of a Diels-Alder reaction. *Nature* **2016**, 531, 88.

(60) Wang, Z.; Danovich, D.; Ramanan, R.; Shaik, S. Oriented-External Electric Fields Create Absolute Enantioselectivity in Diels-Alder Reactions: Importance of the Molecular Dipole Moment. *J. Am. Chem. Soc.* **2018**, 140 (41), 13350−13359.